Dynamic Jahn-Teller effect on the far-infrared spectrum of Fe^{2+} in $Cd_{1-x}Fe_xTe$ compounds

C. Testelin, C. Rigaux, A. Mauger, and A. Mycielski*
Groupe de Physique des Solides, Tour 23, Université Paris VI et VII, 2 place Jussieu, 75251 Paris CEDEX 05, France

C. Julien
Laboratoire de Physique des Solides, Tour 13, Université Paris VI, 2 place Jussieu, 75251 Paris CEDEX 05, France
(Received 13 June 1991; revised manuscript received 9 December 1991)

The optical absorption of substitutional Fe^{2+} ions in $Cd_{1-x}Fe_xTe$ compounds has been measured in the far infrared (10–80 cm^{-1}) at temperatures from 5 to 300 K. Electronic transitions inside the ^5E multiplet of Fe^{2+} are observed at low temperature, but the crystal-field model is not sufficient to explain the experimental features. Calculations of the ^5E electron states are performed, taking into account the Jahn-Teller interaction with the vibrations of the host lattice. The electron-phonon coupling is approximated by a single pair of E modes corresponding to TA(L) phonons. Energies and oscillator strengths for electric- and magnetic-dipole transitions from the ground state to excited levels are calculated within the Jahn-Teller model. An excellent quantitative agreement is obtained with the low-temperature absorption lines for a Jahn-Teller energy of 2.5 cm^{-1}, an effective spin-orbit splitting $\lambda=-101.9$ cm^{-1}, a spin-spin interaction coefficient $\rho=0.18$ cm^{-1}, and a phonon energy of the TA(L) mode (28 ± 0.5 cm^{-1}) quite consistent with the neutron-scattering results. The high-temperature far-infrared absorption spectra give also evidence for a local mode of Fe in CdTe and for a two-phonon process involving the TA(X) mode of CdTe (35 ± 0.5 cm^{-1}).

I. INTRODUCTION

The d^6-electron spectrum of an Fe^{2+} ion in Fe-doped CdTe has been investigated by Slack *et al.*[1,2] through infrared absorption experiments. However, no definitive interpretation of the far-infrared (FIR) optical transitions has been given to date. In a site of tetrahedral symmetry (T_d), the ^5D configuration of the free Fe^{2+} ion is split by the crystal field into an orbital doublet ^5E and triplet $^5T_2$ (separated by $\Delta=10|Dq|$) lying at higher energy. Furthermore, the spin-orbit interaction removes partially the degeneracy of the ^5E ground state which is split into five nearly equidistant levels ($\Gamma_1,\Gamma_4,\Gamma_3,\Gamma_5,\Gamma_2$) separated by about $6\lambda^2/\Delta$, with λ the spin-orbit parameter ($\lambda=-100$ cm^{-1}). Optical transitions from the singlet Γ_1 ground state to levels of $^5T_2$ have been seen near 2.500 cm^{-1}.[1] Transitions among the ^5E spin-orbit-split levels were observed in the FIR region.[2] The lowest-energy line occurring at 18.6 cm^{-1} corresponds to transition $\Gamma_1\rightarrow\Gamma_4$ but the presence of extra lines in the low-temperature absorption spectra is not consistent with the predictions of the simple crystal-field model.[2,3]

The influence of the dynamic Jahn-Teller effect on the ^5E electron states of Fe^{2+} in CdTe was initially studied by Vallin,[4] and more recently by Vogel and Rivera-Iratchet.[5] It was shown that the electron-phonon coupling with E vibrational modes distorts the energy-level spectrum and also may introduce additional electronic transitions among the ^5E multiplet. Unfortunately the energy of the E phonon mode considered in these works is not consistent with the data of neutron-scattering experiments performed in CdTe by Rowe *et al.*[6]

The purpose of the present paper is to report extensive FIR absorption studies in $Cd_{1-x}Fe_xTe$ diluted magnetic semiconductors. Taking into account the lattice-dynamics data,[6] we have determined the influence of the dynamical Jahn-Teller effect on the electronic states of an Fe^{2+} ion and we propose a coherent interpretation of the FIR optical-absorption spectra. Experimental techniques are described in Sec. II. FIR absorption spectra of $Cd_{1-x}Fe_xTe$ measured in the spectral region 10–80 cm^{-1}, at temperatures between 5 and 100 K, are presented in Sec. III. Section IV deals with the theoretical model. The relevant predictions of the crystal-field theory are first summarized. Then we introduce the electron-phonon coupling between ^5E electronic states and a single pair of the E phonon mode to derive the vibronic states. Calculated energies and oscillator strengths for optical transitions are compared with experimental data in Secs. V and VI.

II. EXPERIMENTS

FIR absorption measurements were carried out on single crystals of $Cd_{1-x}Fe_xTe$ in the iron composition range $0\leq x\leq 0.03$. The Fe molar fraction was determined by electron microprobe analysis. The infrared absorption spectra were recorded in the spectral region 10–100 cm^{-1} using a Brucker IFS113 vacuum Fourier transform spectrometer. The low-frequency domain is explored using a 100-μm-thick Mylar beam splitter, a mercury lamp as a source, and the apparatus was carefully isolated from the external vibrations in order to improve the signal-to-noise ratio. A germanium bolometer operating at helium temperature is used as a sensitive detector. Each spectrum is the average of 100 scans with a spectral resolu-

tion of 0.5 cm^{-1}. The FIR absorption spectra were taken for all investigated samples in the temperature range 5–300 K. The low-temperature experiments were carried out using a temperature variable cryostat and the sample temperature was controlled by a silicon diode probe with an accuracy of ±1 K.

III. FAR-INFRARED ABSORPTION SPECTRA

The FIR absorption spectrum of the diluted compound $Cd_{0.99}Fe_{0.01}Te$ at $T=5$ K is illustrated in Fig. 1. The comparison with the spectrum of pure CdTe, reported in the same figure, shows the presence of additional peaks at wave numbers 18.6, 66, and 74 cm^{-1} in the Fe-doped sample. A weaker structure is also observed at 54 cm^{-1}. In order to distinguish absorption peaks attributable to Fe-ion electronic excitation from phonon lines, we have studied the dependence of the spectrum on both the temperature T and the concentration x of Fe^{2+} ions. Figure 2 shows experimental spectra measured at several temperatures for the compound $Cd_{0.99}Fe_{0.01}Te$. The absorption lines at 18.6, 66, and 74 cm^{-1} are weakened when T is increased, and disappear above 20 K. The structure at 54 cm^{-1}, hardly visible at 5 K, is intensified by increasing the temperature and gives rise to an absorption peak occurring at a slightly lower energy (53 cm^{-1} at $T=100$ K). We observe the same temperature behavior for the resonance at 71.5 cm^{-1} which is present also in the spectrum of CdTe. The high-temperature FIR spectrum of $Cd_{1-x}Fe_xTe$ consists of two sharp lines at 53 and 71.5 cm^{-1} (Figs. 2 and 3).

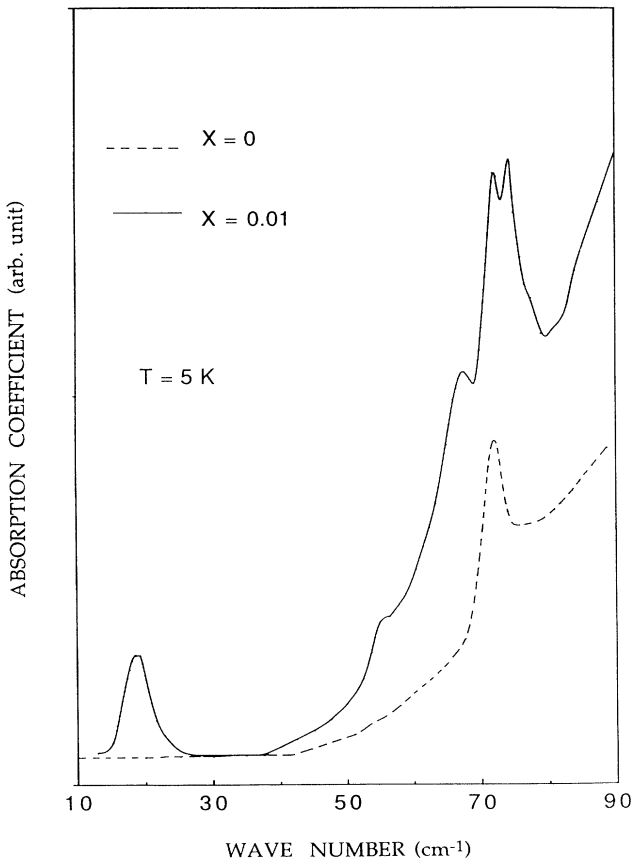

FIG. 1. FIR absorption spectra of CdTe and $Cd_{1-x}Fe_xTe$ ($x=0.01$) at $T=5$ K.

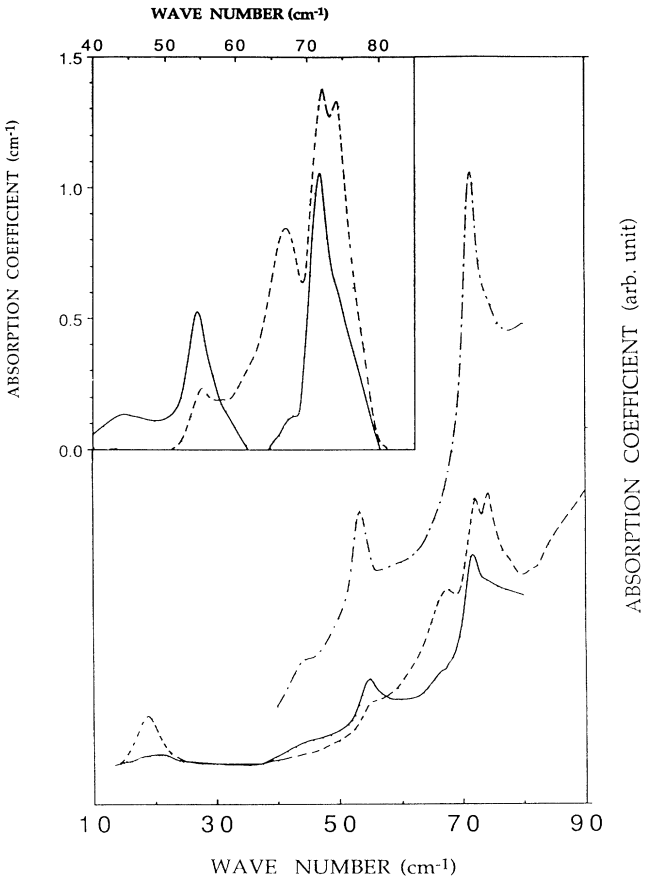

FIG. 2. FIR absorption spectra of $Cd_{0.99}Fe_{0.01}Te$ at $T=5$ K (dashed line), 20 K (solid line), and 90 K (dotted-dashed line). The inset shows the line shape of the spectrum obtained after subtracting the background.

At $T=100$ K, the line shape of the spectra for compounds with iron contents $x=0$, 0.01, and 0.03 is compared in Fig. 3. The absorption at 53 cm^{-1} is clearly stronger in the spectrum of the most concentrated alloy but the intensity of the peak at 71.5 cm^{-1} is comparable in the spectra of CdTe and $Cd_{0.97}Fe_{0.03}Te$.

At 5 K, only the ground state is significantly populated. Therefore, electronic excitations can be observed from the Γ_1 ground state towards excited levels of the ^5E multiplet. Moreover, the intensity of the phonon lines should increase with temperature. According to the observed features, we may assign the low-temperature absorption lines (at 18.6, 66, and 74 cm^{-1}) to electronic transitions originating from the Γ_1 ground state towards excited levels of the ^5E multiplet. The two other lines at 53 and 71.5 cm^{-1} result from phonon absorption processes.

Our present data are quite consistent with the results reported previously by Slack, Roberts, and Vallin[2] for very diluted $Cd_{1-x}Fe_xTe$ alloys. However, our absorp-

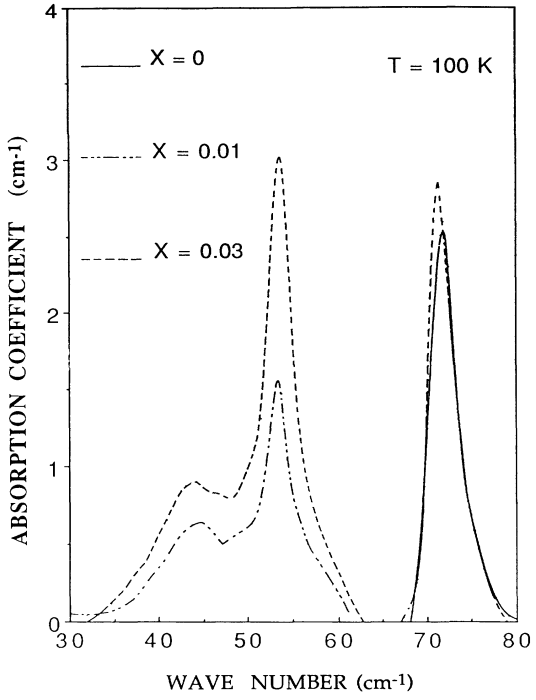

FIG. 3. Line shape of the absorption spectrum at $T=100$ K, in the spectral region 30–80 cm^{-1}, for $Cd_{1-x}Fe_xTe$ ($x=0.01$ and 0.03) and for CdTe, after subtracting the background.

tion measurements do not confirm the presence of two weak structures at wave numbers 36 and 46 cm^{-1} reported by Slack, Roberts, and Vallin[2] in the low-temperature spectra. These features were attributed by Slack, Roberts, and Vallin[2] to single-phonon absorption bands associated with transverse-acoustic modes at the L and X points of the Brillouin zone. However, this assignment is not compatible with the phonon-dispersion relations obtained from neutron-scattering experiments in CdTe:[6] the neutron results for the frequencies of the transverse-acoustic modes correspond to 29 cm^{-1} at the L point and 35 cm^{-1} at the X point, with an accuracy of 5%.

IV. THEORY

The spectrum of $3d^6$ electrons of Fe^{2+} ion CdTe has been intensively investigated.[2–5] We summarize the essential results of the crystal-field theory, which are relevant for the formulation of the Jahn-Teller model developed in Sec. IV B.

A. Crystal-field model

The ground state ^5D ($L=2, S=2$) of the Fe^{2+} free ion is split into an orbital doublet ^5E and an orbital triplet $^5T_2$ by the crystal field of tetrahedral symmetry (point group T_d).[7] The energy separation between the ground state ^5E and $^5T_2$ triplet is $\Delta=10|Dq|=2480$ cm^{-1}. The basis functions for the E and T_2 representations are

TABLE I. Spin-orbit functions appropriate to the Fe^{2+} ion in the symmetry T_d, used as a basis set for the states issuing from the ^5E multiplet.

Irreducible representations	Functions
Γ_2	$\lvert b)=\frac{1}{\sqrt{2}}(\lvert\theta\varepsilon\rangle-\lvert\varepsilon\theta\rangle)$
Γ_5	$\lvert x)=\frac{1}{2}(\sqrt{3}\lvert\varepsilon x\rangle-\lvert\theta x\rangle)$ $\lvert y)=-\frac{1}{2}(\sqrt{3}\lvert\varepsilon y\rangle+\lvert\theta y\rangle)$ $\lvert z)=\lvert\theta z\rangle$
Γ_3	$\lvert\theta)=\frac{1}{\sqrt{2}}(\lvert\varepsilon\varepsilon\rangle-\lvert\theta\theta\rangle)$ $\lvert\varepsilon)=\frac{1}{\sqrt{2}}(\lvert\theta\varepsilon\rangle+\lvert\varepsilon\theta\rangle)$
Γ_4	$\lvert u)=-\frac{1}{2}(\sqrt{3}\lvert\theta x\rangle+\lvert\varepsilon x\rangle)$ $\lvert v)=\frac{1}{2}(\sqrt{3}\lvert\theta y\rangle-\lvert\varepsilon y\rangle)$ $\lvert w)=\lvert\varepsilon z\rangle$
Γ_1	$\lvert a)=\frac{1}{\sqrt{2}}(\lvert\theta\theta\rangle+\lvert\varepsilon\varepsilon\rangle)$

TABLE II. Spin-orbit functions appropriate to the Fe^{2+} ion in the symmetry T_d, used as a basis set for the states issuing from the $^5T_2$ multiplet.

Irreducible representations	Functions
Γ_1	$\lvert A)=\frac{1}{\sqrt{3}}(\lvert xx\rangle+\lvert yy\rangle+\lvert zz\rangle)$
Γ_4	$\lvert U')=\frac{1}{2\sqrt{3}}(\sqrt{3}\lvert x\theta\rangle+\lvert x\varepsilon\rangle+2\lvert zy\rangle-2\lvert yz\rangle)$ $\lvert V')=\frac{1}{2\sqrt{3}}(-2\lvert zx\rangle-\sqrt{3}\lvert y\theta\rangle+\lvert y\varepsilon\rangle+2\lvert xz\rangle)$ $\lvert W')=\frac{1}{\sqrt{3}}(\lvert yx\rangle-\lvert xy\rangle-\lvert z\varepsilon\rangle)$
Γ_5	$\lvert X')=\frac{1}{2\sqrt{5}}(\sqrt{3}\lvert x\theta\rangle-3\lvert x\varepsilon\rangle+2\lvert zy\rangle+2\lvert yz\rangle)$ $\lvert Y')=\frac{1}{2\sqrt{5}}(-2\lvert zx\rangle-\sqrt{3}\lvert y\theta\rangle-3\lvert y\varepsilon\rangle-2\lvert xz\rangle)$ $\lvert Z')=\frac{1}{\sqrt{5}}(\lvert yx\rangle+\lvert xy\rangle-\sqrt{3}\lvert z\theta\rangle)$
Γ_3	$\lvert\Theta)=\frac{1}{\sqrt{6}}(\lvert xx\rangle+\lvert yy\rangle-2\lvert zz\rangle)$ $\lvert E)=\frac{1}{\sqrt{2}}(-\lvert xx\rangle+\lvert yy\rangle)$
Γ_4	$\lvert U)=\frac{1}{\sqrt{6}}(-\sqrt{3}\lvert x\theta\rangle-\lvert x\varepsilon\rangle-\lvert yz\rangle+\lvert zy\rangle)$ $\lvert V)=\frac{1}{\sqrt{6}}(-\lvert zx\rangle+\sqrt{3}\lvert y\theta\rangle-\lvert y\varepsilon\rangle+\lvert xz\rangle)$ $\lvert W)=\frac{1}{\sqrt{6}}(-\lvert xy\rangle+\lvert yx\rangle+2\lvert z\varepsilon\rangle)$
Γ_5	$\lvert X)=\frac{1}{\sqrt{10}}(-\lvert x\theta\rangle+\sqrt{3}\lvert x\varepsilon\rangle+\sqrt{3}\lvert yz\rangle+\sqrt{3}\lvert zy\rangle)$ $\lvert Y)=\frac{1}{\sqrt{10}}(-\sqrt{3}\lvert zx\rangle+\sqrt{3}\lvert y\varepsilon\rangle-\sqrt{3}\lvert xz\rangle+\lvert y\theta\rangle)$ $\lvert Z)=\frac{1}{\sqrt{10}}(\sqrt{3}\lvert xy\rangle+\sqrt{3}\lvert yx\rangle+2\lvert z\theta\rangle)$

$$|\theta\rangle = Y_2^0 \quad \text{and} \quad |\varepsilon\rangle = \frac{Y_2^2 + Y_2^{-2}}{\sqrt{2}} \quad (E \text{ symmetry});$$

$$|x\rangle = \frac{Y_2^1 + Y_2^{-1}}{i\sqrt{2}}, \quad |y\rangle = \frac{Y_2^{-1} - Y_2^{-1}}{\sqrt{2}}, \quad |z\rangle = \frac{Y_2^2 - Y_2^{-2}}{i\sqrt{2}}$$

(T_2 symmetry) ; (4.1)

where Y_2^m ($m = 0, \pm 1, \pm 2$) are spherical harmonics. Each orbital function is fivefold degenerate due to the spin $S = 2$ of $3d^6$ electrons.

The spin-orbit interaction $H_{s.o.} = \lambda \mathbf{L}\cdot\mathbf{S}$ partially removes the degeneracy of ^5E and $^5T_2$ multiplets. Since the spin functions $S = 2$ span the irreducible representations $\Gamma_3 + \Gamma_5$, the T_d group multiplication table gives[4,8]

$$\Gamma_3 \times (\Gamma_3 + \Gamma_5) = \Gamma_1 + \Gamma_2 + \Gamma_3 + \Gamma_4 + \Gamma_5 \quad \text{for } ^5E ,$$

$$\Gamma_5 \times (\Gamma_3 + \Gamma_5) = \Gamma_1 + \Gamma_3 + 2\Gamma_4 + 2\Gamma_5 \quad \text{for } ^5T_2 .$$

The orbital states ^5E yield five irreducible representations while the $^5T_2$ triplet yields six. The explicit spin-orbit wave functions for the 25 individual levels are reported in Tables I and II. The wave functions are linear combinations of products of orbital with spin states, denoted $|ij\rangle$, where $|i\rangle$ and $|j\rangle$ refer to orbital and spin functions, respectively (i and j run independently over $\theta, \varepsilon, x, y, z$).

The spin-orbit interaction does not couple states belonging to different irreducible representations but induces a mixing between ^5E and $^5T_2$ terms.

For completeness, the magnetic spin-spin interaction among the electrons of an Fe^{2+} ion is introduced:

$$H_{ss} = -\rho\{(\mathbf{L}\cdot\mathbf{S})^2 + \tfrac{1}{2}\mathbf{L}\cdot\mathbf{S}\} . \tag{4.2}$$

The energy spectrum of the ^5E and $^5T_2$ states is then obtained by expressing the total Hamiltonian including the crystal field, the spin-orbit, and spin-spin interactions in the basis of the spin-orbit wave functions (Tables I and II). The 25×25 matrix is decoupled into two 2×2, six 3×3, and one 1×1 blocks. For each irreducible representation, these matrices are

$$\Gamma_1: \quad \begin{pmatrix} 6Dq - 24\rho & -2\sqrt{6}\lambda - 3\sqrt{6}\rho \\ -2\sqrt{6}\lambda - 3\sqrt{6}\rho & -4Dq - 2\lambda - 27\rho \end{pmatrix} \quad \text{for } [|a\rangle, |A\rangle] , \tag{4.3a}$$

$$\Gamma_3: \quad \begin{pmatrix} 6Dq - 12\rho & 2\sqrt{3}\lambda - 3\sqrt{3}\rho \\ 2\sqrt{3}\lambda - 3\sqrt{3}\rho & -4Dq + \lambda - \frac{27}{2}\rho \end{pmatrix} \quad \text{for } [|\theta\rangle, |\Theta\rangle] \text{ and } [|\varepsilon\rangle, |E\rangle] , \tag{4.3b}$$

$$\Gamma_4: \quad \begin{pmatrix} 6Dq - 18\rho & \sqrt{6}\lambda - \frac{3}{2}\sqrt{6}\rho & -2\sqrt{3}\lambda - 3\sqrt{3}\rho \\ \sqrt{6}\lambda - \frac{3}{2}\sqrt{6}\rho & -4Dq + \lambda - \frac{15}{2}\rho & 6\sqrt{2}\rho \\ -2\sqrt{3}\lambda - 3\sqrt{3}\rho & 6\sqrt{2}\rho & -4Dq - 2\lambda - 15\rho \end{pmatrix}$$

$$\text{for } [|u\rangle, |U\rangle, |U'\rangle], \ [|v\rangle, |V\rangle, |V'\rangle], \text{ and } [|w\rangle, |W\rangle, |W'\rangle] , \tag{4.3c}$$

$$\Gamma_5: \quad \begin{pmatrix} 6Dq - 6\rho & \sqrt{\frac{18}{5}}\lambda - \frac{7}{2}\sqrt{\frac{18}{5}}\rho & -\sqrt{\frac{12}{5}}\lambda - \frac{3}{2}\sqrt{\frac{12}{5}}\rho \\ \sqrt{\frac{18}{5}}\lambda - \frac{7}{2}\sqrt{\frac{18}{5}}\rho & -4Dq + 3\lambda - \frac{141}{10}\rho & \frac{6\sqrt{6}}{5}\rho \\ -\sqrt{\frac{12}{5}}\lambda - \frac{3}{2}\sqrt{\frac{12}{5}}\rho & \frac{6\sqrt{6}}{5}\rho & -4Dq - 2\lambda - \frac{27}{5}\rho \end{pmatrix}$$

$$\text{for } [|x\rangle, |X\rangle, |X'\rangle], \ [|y\rangle, |Y\rangle, |Y'\rangle] \text{ and } [|z\rangle, |Z\rangle, |Z'\rangle] . \tag{4.3d}$$

For Γ_2, we have only a 1×1 matrix corresponding to the state $|b\rangle$ at an energy $6Dq$. For $\rho = 0$, these matrices are identical to those reported in Ref. 2.

The ground multiplet ^5E is split into five levels: Γ_1 (singlet), Γ_4 (triplet), Γ_3 (doublet), Γ_5 (triplet), and Γ_2 (singlet), whose eigenfunctions and eigenenergies are obtained exactly by the diagonalization of the matrices (4.3) for a given set of parameters Δ, λ, and ρ. We denote $|\tilde{e}\rangle$ the eigenfunction built from the spin-orbit function $|e\rangle$ plus a small admixture of the $^5T_2$ wave functions (Tables I and II). The mixing coefficients are determined for each set of parameters. As we will see later (Sec. V), the ^5E-$^5T_2$ mixing induced by the spin-dependent terms is essential for the interpretation of the optical transitions inside the ^5E multiplet.

B. Jahn-Teller coupling

The interaction between the electrons of Fe^{2+} ions and lattice vibrations of the crystal results in changes of the crystal field induced by the atomic displacements. This interaction can be expanded as a power series of normal displacements Q_s.[9] Usual approximations amount to truncate the series to the second-order terms (in Q_s, $Q_{s'}$). Moreover, only the diagonal elements ($s = s'$) are retained, so that Q_s can be viewed as the normal coordi-

nates of the vibration modes of the lattice. In such a case, the electron-phonon interaction is reduced to the linear-in-Q terms:

$$H_{JT}=\sum_s (\partial H/\partial Q_s)Q_s \ . \tag{4.4}$$

H is the electronic Hamiltonian at the equilibrium position of the atoms. The suffix s runs over θ,ε and ξ,η,ζ to label vibration modes belonging to the E and T_2 representations of T_d, respectively.

The general form of the Jahn-Teller matrix interaction has been derived for states of each representation in terms of the normal modes.[10] In order to determine the Jahn-Teller effect on the ten lowest energy levels of the ^5E multiplet, we neglect E-T and T-T electron-phonon coupling terms arising primarily from the admixture of the $^5T_2$ contribution into the spin-orbit electronic wave functions. We retain only the coupling between the vibrational modes of E symmetry and the dominant E terms of the spin-orbit wave functions $|\tilde{e}\rangle$. The same treatment was initially used by Vallin.[4]

Within the approximation the Jahn-Teller coupling with the ^5E orbital states may be described by a single pair of terms involving both Q_θ and Q_ε modes corresponding to the E representation,

$$H_{JT}=V(Q_\theta D_\theta+Q_\varepsilon D_\varepsilon) \ , \tag{4.5}$$

where D_θ and D_ε are dimensionless operators acting on the orbital components $|\theta\rangle$ and $|\varepsilon\rangle$ of the electronic wave functions[11]

$$D_\theta: \begin{bmatrix} -1 & 0 \\ 0 & 1 \end{bmatrix}; \ D_\varepsilon: \begin{bmatrix} 0 & 1 \\ 1 & 0 \end{bmatrix} . \tag{4.6}$$

We will find that the Jahn-Teller energy is much smaller than the zero point energy of acoustic phonons at the Brillouin-zone boundaries, so that the Jahn-Teller potential is not binding. Since this is a pure quantum-mechanical effect, a classical treatment of Eq. (4.5) is not pertinent. We thus express Eq. (4.5) in a second-quantization notation, which amounts to replacing Q_θ,Q_ε by the corresponding displacement operators proportional to $a_s^\dagger+a_s$, with $s=\theta,\varepsilon$ while $a_s^\dagger,a_s$ are creation and annihilation operators of a phonon of symmetry s. We then find

$$H_{JT}=K[D_\theta(a_\theta^\dagger+a_\theta)+D_\varepsilon(a_\varepsilon^\dagger+a_\varepsilon)] \ , \tag{4.7}$$

where K is a coupling constant. In the harmonic approximation, the vibrational Hamiltonian is

$$H_{vib}=\hbar\omega(a_\theta^\dagger a_\theta+a_\varepsilon^\dagger a_\varepsilon+1) \ . \tag{4.8}$$

We assume that all the E phonons have the same energy. This, of course, is an approximation, since all the E phonons along their dispersion curves in the Brillouin zone should contribute, in principle. It is the Einstein approximation, which approximates the spectral phonon density by a Dirac peak at the Brillouin-zone boundary. Moreover, only acoustic phonons are of interest. The optical phonons have energies much higher than those of the Fe^{2+} electronic excitations, and thus cannot interact efficiently with them. The symmetry of the phonons in the zinc-blende lattice has been studied by Loudon,[12] who gave the decomposition of the space group T_d for each phonon at the X and L points of the Brillouin zone. According to this work, among the zone boundary phonons, only the TA(L) phonon satisfies the E symmetry. $\hbar\omega$ in Eq. (4.8) is thus the energy of this TA(L) phonon.

C. Determination of the vibronic states

We consider the Hamiltonian

$$H'=H+H_{JT}+H_{vib} \tag{4.9}$$

with H the electronic Hamiltonian, H_{JT} and H_{vib} being given in Eqs. (4.7) and (4.8). For $K=0$, the unperturbed eigenstates of H' are products $|\tilde{e},nm\rangle$ of an electronic wave function $|\tilde{e}\rangle$ by the vibrational function $|nm\rangle$ characterized by the eigenvalues n and m of $a_\theta^\dagger a_\theta$ and $a_\varepsilon^\dagger a_\varepsilon$, respectively.

As $K\neq 0$, each electronic state $|\tilde{e},nm\rangle$ is coupled to an infinite sequence of states $|\tilde{e}',n'm'\rangle$ involving electronic functions of different symmetry and of different quantum numbers $n',m'=0,1,2,\ldots$. These states $|\tilde{e}',n'm'\rangle$ are generated by successive applications of H_{JT} on initial states $|\tilde{e},00\rangle$. The matrix Hamiltonian is then expressed in this basis, making use of the relations

$$a_\theta^\dagger|nm\rangle=\sqrt{n+1}\,|n+1,m\rangle \ ,$$

$$a_\varepsilon^\dagger|nm\rangle=\sqrt{m+1}\,|n,m+1\rangle \ ,$$

$$a_\theta|nm\rangle=\sqrt{n}\,|n-1,m\rangle, \quad a_\varepsilon|nm\rangle=\sqrt{m}\,|n,m-1\rangle \ .$$

Let us take the example of the ground electronic state $|\tilde{a},00\rangle$ to illustrate the procedure. The electronic function is $|\tilde{a}\rangle=a_1|a\rangle+b_1|A\rangle$, with $|a\rangle$ and $|A\rangle$ given in Tables I and II. The application of H_{JT} to this state is

$$H_{JT}|\tilde{a},00\rangle=a_1a_2K\sqrt{2}\left[\frac{|\tilde{\theta},10\rangle+|\tilde{\varepsilon},01\rangle}{\sqrt{2}}\right] , \tag{4.10}$$

which generates the normalized new vibronic state in parentheses, with $|\tilde{\theta}\rangle=a_2|\theta\rangle+b_2|\Theta\rangle$. Then, H_{JT} can be applied to this new vibronic state to generate another one, etc. Equation (4.10) shows that H_{JT} couples a spin-orbit function of symmetry Γ_1 to a spin-orbit function of symmetry Γ_3. Successive applications of H_{JT} will further couple these states to spin-orbit functions of symmetry Γ_2, but not to those of symmetry Γ_4 and Γ_5. The same procedure has to be applied to zero-phonon states $|\tilde{e},00\rangle$ with $|\tilde{e}\rangle$ states of Γ_4 and Γ_5 symmetry. Successive applications of H_{JT} to the three sets of basis functions $[|\tilde{u},00\rangle,|\tilde{x},00\rangle]$, $[|\tilde{v},00\rangle,|\tilde{y},00\rangle]$, and $[|\tilde{w},00\rangle,|\tilde{z},00\rangle]$ will also generate diagonal blocks for H'. At this stage, we have thus reduced the H' matrix in four diagonal blocks, for which the eigenvalue problem can be solved separately. We denote $|\Gamma_k:\Gamma_l,nm\rangle$ the eigenstate of the H' matrix which reduces to $|\Gamma_l,nm\rangle$ in the limit $K=0$ and which is generated by the application of H_{JT} on the initial state $|\Gamma_k,00\rangle$. The vibronic function $|\Gamma_k:\Gamma_l,nm\rangle$ has the symmetry Γ_k.

In practice, we only apply H_{JT} to the zero-phonon

states a finite number N of times, i.e., the basis set is determined by the decomposition of $H_{\rm JT}^{N}|\bar{e},00)$ inside each block. Note that $H_{\rm JT}^{N+1}|\bar{e},00)$ only introduces new states $|\bar{e},n'm')$ with $n'+m'=N+1$ with respect to the previous step N. Therefore, the limit to N means that the coupling of the $|\bar{e},nm)$ states with states $|\bar{e}',n'm')$ is treated exactly, up to $n'+m'=N$ phonons. In the energy range explored in the absorption spectra, only vibronic states with $n+m\leq 2$ can be excited. We thus choose N in such a way that a good description of these vibronic states is achieved. The convergence for both the eigenstates and the eigenvalues of these modes is actually very fast, and we found that it is fully achieved for $N=6$. For this particular value of N, the block associated with $|\bar{a},00)$ in H' is a 12×12 matrix; the three other ones associated with the Γ_4 and Γ_5 symmetries are 49×49 matrices (which can even be reduced in 24×24 and 25×25 subsets).[13] Indeed, the dimensions of these matrices are small enough so that the eigenvalue problem is easily solved on the computer.

V. OPTICAL TRANSITIONS

A. General formulation

The selection rules for optical transitions are obtained from the nonvanishing matrix elements $\langle F|\mathbf{O}|I\rangle$ of the transition operator $\mathbf{O}$ between initial (I) and final (F) levels. For magnetic-dipole transitions, $\mathbf{O}$ is the component of the electron magnetic moment $\mathbf{M}=\mathbf{L}+2\mathbf{S}$ along the magnetic field of the radiation. For electric-dipole transition, $\mathbf{O}$ is $\mathbf{R}=\sum\mathbf{r}_i$ the sum of the d-electron position vectors in the direction of light polarization.

The absorption coefficient $\alpha(\nu)$ resulting from the transition $I\rightarrow F$ is given by[14]

$$\alpha(\nu)=\frac{\pi Ne^2h}{mcn}\left[\frac{\varepsilon_{\rm eff}}{\varepsilon}\right]^2 d_I\left[\frac{x_I}{d_I}-\frac{x_F}{d_F}\right]f(I,F)\times\delta(E_F-E_I-h\nu)\ . \tag{5.1}$$

N is the number of Fe^{2+} ions per unit volume. d_I and d_F denote the degeneracy of the levels I,F, the occupancy factors of which are x_I and x_F, respectively. n is the refraction index, m is the electron mass, and c is the light velocity. $\varepsilon_{\rm eff}/\varepsilon$ is the ratio of the electric field at the Fe^{2+} site to the average macroscopic field in the crystal. This ratio is approximated by $(n^2+2)/3$.[14] The oscillator strengths $f(I,F)$ for magnetic and electric transitions are[15]

$$f_m(I,F)=\frac{E_{IF}n^2}{2mc^2d_I}\left[\frac{\varepsilon}{\varepsilon_{\rm eff}}\right]^2\sum_{i,f}|\langle Ff|(\mathbf{L}+2\mathbf{S})\cdot(\mathbf{e}\Lambda\mathbf{k})|Ii\rangle|^2 \tag{5.2}$$

$$f_e(I,F)=\frac{2mE_{IF}}{h^2d_I}\sum_{i,f}|\langle Ff|\mathbf{R}\cdot\mathbf{e}|Ii\rangle|^2\ , \tag{5.3}$$

where the sum runs over the i and f eigenstates of the degenerate initial and final levels, respectively. $\mathbf{k}$ and $\mathbf{e}$ are unit vectors in the directions of the light propagation and polarization, respectively. $E_{IF}=E_F-E_I$ is the transition energy.

B. Case $K=0$

Optical transition among the ^5E multiplet result from both electric- and magnetic-dipole processes. Electric-dipole transitions between pure orbital E states are forbidden by symmetry. The spin-orbit mixing between the ^5E and $^5T_2$ states is responsible for the excitation of electric-dipole transitions among the ^5E multiplet. To get a numerical estimate of the oscillator strengths, we need numerical values for Dq, λ, and ρ. The parameter Dq has been measured accurately:[1] $Dq=-248\ \text{cm}^{-1}$. The value of ρ was determined by Watson and Blume:[16] $\rho=0.18\ \text{cm}^{-1}$. The lowest-energy absorption peak at $18.6\ \text{cm}^{-1}$ in the FIR spectrum corresponds to the $\Gamma_1\rightarrow\Gamma_4$ transition. This allows us to determine the value of λ, once Dq and ρ are fixed: $\lambda=-97.7\ \text{cm}^{-1}$.

We have computed the mixing coefficients entering the expression of the wave functions $|\bar{e}\rangle$. The eigenenergies for the electronic levels originating from the ^5E multiplet are shown in Fig. 4, for above values of Dq, λ, and ρ. Numerical values of the oscillator strengths are then obtained for magnetic transitions, from Eq. (5.2), and are also reported in Fig. 4. For electric transitions which arise from ^5E-$^5T_2$ spin-orbit mixing, all oscillator strengths in Eq. (5.3) are expressed in terms of a unique matrix element $\langle\theta|R_z|z\rangle$ between orbital wave functions of ^5E and $^5T_2$ states. The values of the oscillator strengths for electric-dipole transitions reported in Fig. 4 have been obtained for $|\langle\theta|R_z|z\rangle|=0.06$ Å. Besides the magnetic-dipole transition $\Gamma_1\rightarrow\Gamma_4$ at $18.6\ \text{cm}^{-1}$, the

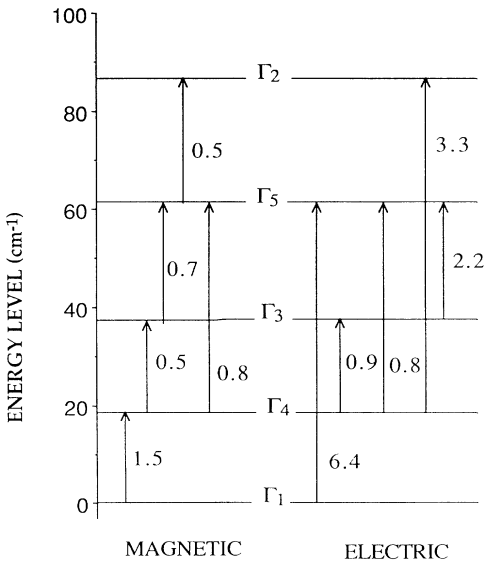

FIG. 4. Allowed optical transitions (arrows) among the spin-orbit ^5E levels of Fe^{2+} in CdTe induced by the electric- and magnetic-dipole processes. The number reported on each arrow is the oscillator strength times 10^8 calculated from the crystal-field model using Eqs. (5.2) and (5.3) with $Dq=-248\ \text{cm}^{-1}$, $\rho=0.18\ \text{cm}^{-1}$, and $\lambda=-97.7\ \text{cm}^{-1}$.

TABLE III. Vibronic eigenstates of the Hamiltonian in the presence of a Jahn-Teller coupling, obtained for the choice of parameters reported in Eq. (6.1) of the text. These states are expressed in the basis $|\bar{e},nm)$. The terms having coefficients smaller in magnitude than 0.05 are omitted in the expansion.

$$|\Gamma_1{:}\bar{a},00)=0.9850|\bar{a},00)-0.1686\frac{|\bar{\theta},10)+|\bar{\varepsilon},01)}{\sqrt{2}}$$

$$|\Gamma_4{:}\bar{w},00)=0.9541|\bar{w},00)-0.2742|\bar{w},10)+0.1031|\bar{z},01)+0.0561|\bar{w},20)$$

$$|\Gamma_4{:}\bar{w},10)=0.8753|\bar{w},10)-0.3704|\bar{w},20)+0.2682|\bar{w},00)-0.1000|\bar{z},11)+0.0941|\bar{w},30)+0.0662|\bar{z},01)$$

$$|\Gamma_5{:}\bar{w},01)=0.9113|\bar{w},01)+0.3052|\bar{z},00)-0.2329|\bar{w},11)+0.1354|\bar{z},02)$$

$$|\Gamma_4{:}\bar{w},20)=0.7988|\bar{w},20)-0.4319|\bar{w},30)+0.3603|\bar{w},10)+0.1282|\bar{w},40)+0.0990|\bar{z},11)+0.0975|\bar{z},21)+0.0513|\bar{w},00)-0.0500|\bar{w},02)$$

$$|\Gamma_4{:}\bar{w},02)=0.8888|\bar{w},02)+0.3598|\bar{z},01)-0.2108|\bar{w},12)+0.1586|\bar{z},03)-0.0641|\bar{w},00)$$

$$|\Gamma_5{:}\bar{w},11)=0.6877|\bar{w},11)-0.5203|\bar{z},00)+0.3491|\bar{w},01)-0.3069|\bar{w},21)+0.1164|\bar{z},12)+0.1156|\bar{z},02)+0.0783|\bar{w},31)-0.0509|\bar{w},03)$$

$$|\Gamma_5{:}\bar{z},00)=0.7446|\bar{z},00)+0.5200|\bar{w},11)+0.3605|\bar{z},10)-0.1526|\bar{w},21)-0.1103|\bar{w},01)+0.0701|\bar{z},12)+0.0537|\bar{z},20)$$

crystal-field model predicts that there is only one other allowed electronic transition originating from the ground state, namely the electric-dipole transition $\Gamma_1\rightarrow\Gamma_5$ at 61.6 cm^{-1}.

This is contrast with the evidence of two electronic transitions at 66 and 74 cm^{-1} in the low-temperature FIR spectra. Therefore, the crystal-field model is not sufficient to explain the optical transitions.

C. Case $K\neq 0$

In the presence of the Jahn-Teller coupling the vibronic wave functions result from admixture of electronic states Γ_i of different symmetry associated to different vibrational states. The Jahn-Teller interaction makes possible the excitation of transitions involving changes of vibrational states between initial and final vibronic states. We are only interested in electronic transitions originating from the ground state, as only this state is populated at the low temperatures where we have observed the FIR absorption lines involving Fe^{2+} ion excitations. The optical transitions originating from this ground state $|\Gamma_1{:}\Gamma_1 00)$ are readily calculated as a function of the model parameters. The quantum mixing of electronic and vibration states in the constitution of the vibronic states (Table III) have dramatic consequences on the intensity of the optical-absorption lines. While the dominant transitions of the spectrum remain zero-phonon transitions $|\Gamma_1{:}\Gamma_1 00)\rightarrow|\Gamma_4{:}\Gamma_4 00)$ (magnetic) and $|\Gamma_1{:}\Gamma_1 00)\rightarrow|\Gamma_5{:}\Gamma_5 00)$ (electric), the Jahn-Teller coupling makes possible the occurrence of the one-phonon transitions $|\Gamma_1{:}\Gamma_1 00)\rightarrow|\Gamma_5{:}\Gamma_4 01)$, $|\Gamma_1{:}\Gamma_1 00)\rightarrow|\Gamma_4{:}\Gamma_4 10)$, as well as two-phonon transitions $|\Gamma_1{:}\Gamma_1 00)\rightarrow|\Gamma_4{:}\Gamma_4 02)$, $|\Gamma_1{:}\Gamma_1 00)\rightarrow|\Gamma_5{:}\Gamma_4 11)$, $|\Gamma_1{:}\Gamma_1 00)\rightarrow|\Gamma_4{:}\Gamma_4 20)$. The occurrence of one- and two-phonon transitions between the vibronic states is evidenced in Table III by their decomposition on the basis of unperturbed states.

VI. RESULTS AND DISCUSSION

For a quantitative interpretation of the low-temperature absorption lines, we have calculated within the Jahn-Teller model the energies and the oscillator strengths of the optical transitions from the ground state $|\Gamma_1{:}\Gamma_1 00)$ as a function of K, $\hbar\omega$, and λ. We have taken $Dq=-248$ cm^{-1} and $\rho=0.18$ cm^{-1}. Using the experimental value of the energy for the transverse-acoustic phonon at the L point,[6] we have allowed $\hbar\omega$ to vary within a small range, with 29 cm^{-1} as the upper limit.

The assignment of the peak at 18.6 cm^{-1} to the transition $|\Gamma_1{:}\Gamma_1 00)\rightarrow|\Gamma_4{:}\Gamma_4 00)$ imposes a condition between the spin-orbit parameter λ and the Jahn-Teller constant K, implying a decrease of λ (i.e., an increase of $|\lambda|$ as K increases).

Figures 5(a) and 5(b) show the transition energies of vibronic states between the $|\Gamma_4,00)$ and $|\Gamma_5,00)$ states and the ground state, as a function of the Jahn-Teller constant for $\hbar\omega=28$ cm^{-1}. The electric-dipole transition $|\Gamma_1{:}\Gamma_1 00)\rightarrow|\Gamma_5{:}\Gamma_5 00)$, starting from 61.5 cm^{-1} for $K=0$, increases with K and exhibits a maximum around 65.5 cm^{-1}, in agreement with the experimental line position. The Jahn-Teller constant $K=8.4$ cm^{-1} corresponds to this maximum for $\hbar\omega=28$ cm^{-1}.

The analysis of the intensities performed for these values of the parameters predicts that transitions towards $|\Gamma_4{:}\Gamma_4 02)$ and $|\Gamma_4{:}\Gamma_4 20)$ are much weaker (by at least two orders of magnitude) than $|\Gamma_1{:}\Gamma_1 00)\rightarrow|\Gamma_4{:}\Gamma_4 00)$. In contrast, the transition $|\Gamma_1{:}\Gamma_1 00)\rightarrow|\Gamma_5{:}\Gamma_4 11)$ may have comparable strength as $|\Gamma_1{:}\Gamma_1 00)\rightarrow|\Gamma_5{:}\Gamma_5 00)$. Accordingly we assign the experimental line at 74 cm^{-1} to $|\Gamma_1{:}\Gamma_1 00)\rightarrow|\Gamma_5{:}\Gamma_4 11)$. The best agreement between calculated and experimental energies of both $|\Gamma_1{:}\Gamma_1 00)\rightarrow|\Gamma_5{:}\Gamma_5 00)$ and $|\Gamma_1{:}\Gamma_1 00)\rightarrow|\Gamma_5{:}\Gamma_4 11)$ transitions is achieved for the set of parameters

$$K=8.4\pm0.3\ cm^{-1},\quad \lambda=-101.9\pm0.5\ cm^{-1},$$
$$\rho=0.18\ cm^{-1},\quad \hbar\omega=28\pm0.5\ cm^{-1}, \tag{6.1}$$
$$E_{JT}=\frac{K^2}{\hbar\omega}=2.5\pm0.3\ cm^{-1},$$

as shown in Fig. 5. The fact that the electric-dipole transition $|\Gamma_1{:}\Gamma_1 00)\rightarrow|\Gamma_5{:}\Gamma_5 00)$ goes through a maximum, while the $|\Gamma_1{:}\Gamma_1 00)\rightarrow|\Gamma_5{:}\Gamma_4 11)$ transition goes through a minimum, reflects the anticrossing of the $|\Gamma_5{:}\Gamma_5 00)$ and the $|\Gamma_5{:}\Gamma_4 11)$ vibronic states as K varies. The set of parameters in Eq. (6.1) corresponds to a situation close to these extrema, i.e., close to the anticrossing region where

the quantum mixing between $|\Gamma_5{:}\Gamma_5 00)$ and $|\Gamma_5{:}\Gamma_4 11)$ is maximum. This is shown in Table III, where we have reported the mixing coefficients entering the decomposition of the vibronic states in the $|\tilde{e},nm)$ basis. The component of the vibronic state $|\Gamma_5{:}\tilde{w}11)$ on the zero-phonon unperturbed state $|\tilde{z}00)$ (-0.5192) is of the same order as the component of $|\Gamma_5{:}\tilde{z}00)$ (0.7453). This explains why a comparable strength is found for the electric transitions $|\Gamma_1{:}\Gamma_1 00)\rightarrow|\Gamma_5{:}\Gamma_5 00)$ and $|\Gamma_1{:}\Gamma_1 00)\rightarrow|\Gamma_5{:}\Gamma_4 11)$. One can note that the spin-orbit parameter λ $(-101.9\pm0.5$ $\mathrm{cm}^{-1})$ has a value in very good agreement with the determination of the free-ion spin-orbit constant, $\lambda=-103\pm2$ cm^{-1}.[17]

For a complete analysis of the low-temperature absorption data, we have determined the intensities of the optical transitions using the set of parameters in Eq. (6.1). The oscillator strengths of magnetic- and electric-dipole transitions between vibronic states are calculated from Eqs. (5.2) and (5.3). Absolute values of f_m are obtained for magnetic transitions. The oscillator strengths f_e for all electric-dipole transition are expressed in terms of the matrix element $\langle\theta|R_z|z\rangle$ which can be evaluated from the comparison of the line intensities: the ratio f_e/f_m between the strengths of the electric $|\Gamma_1{:}\Gamma_1 00)$ $\rightarrow|\Gamma_5{:}\Gamma_5 00)$ and magnetic $|\Gamma_1{:}\Gamma_{00})\rightarrow|\Gamma_4{:}\Gamma_4 00)$ transitions is estimated by comparing the ratio of the integrated absorption intensities $\int\alpha(\nu)d\nu$ of experimental lines at 66 and 18.6 cm^{-1}, with the theoretical value deduced from Eqs. (5.1)–(5.3). From the absolute strength f_e, we deduce the matrix element $|\langle\theta|R_z|z\rangle|=0.06\pm0.01$ Å. This value is in excellent agreement with the experimental result (0.07 Å) obtained by Slack, Ham, and Chrenko[1] from the analysis of ${}^5E\rightarrow{}^5T_2$ optical transitions in the near-infrared region. The energies and the oscillator strengths for all electric- and magnetic-dipole transitions occurring in the investigated spectral region are reported in Table IV. An excellent agreement is found between theory and experiment. In particular, the presence of the three intense absorption lines at 18.6, 66, and 74 cm^{-1} in the low-temperature FIR spectra is well accounted for by the Jahn-Teller model. The lines at 18.6 and 66 cm^{-1} correspond, respectively, to the magnetic- and electric-dipole transitions originating from the ground state towards Γ_4 and Γ_5 zero-phonon vibronic levels. The most striking feature of the FIR spectrum is the occurrence of the $|\Gamma_1{:}\Gamma_1 00)\rightarrow|\Gamma_5{:}\Gamma_4 11)$ electric-dipole transition at 74

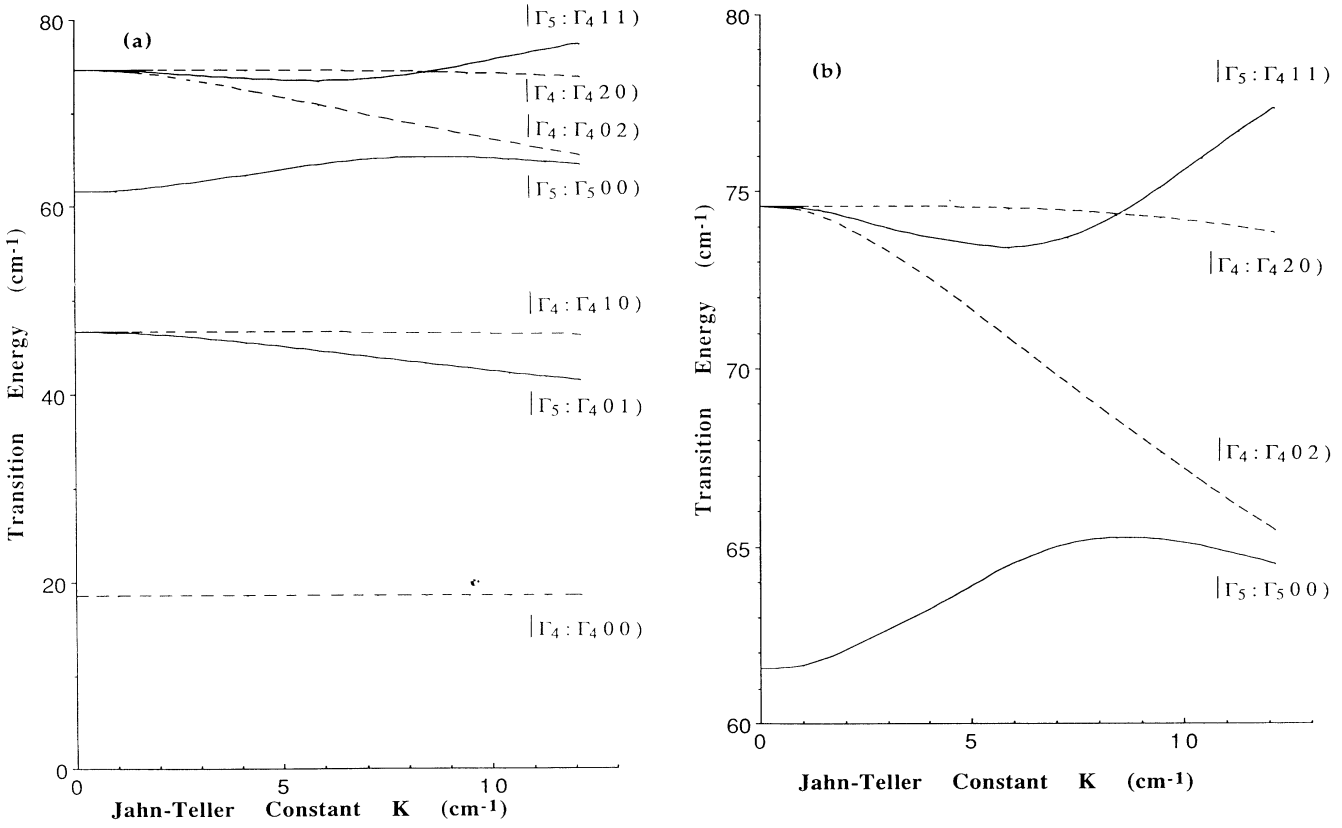

FIG. 5. (a) Energies of allowed transitions originating from the ground state $|\Gamma_1{:}\Gamma_1 00)$ as a function of the Jahn-Teller constant K for the model parameters $\Delta=2480$ cm^{-1}; $\hbar\omega=28$ cm^{-1}; $\rho=0.18$ cm^{-1}. For each value of K, the spin-orbit parameter λ is adjusted in order to keep the lowest-energy transition at 18.6 cm^{-1}. For each transition, the final vibronic state is indicated on each curve. The curves associated with Γ_4 symmetry states are dashed; for the Γ_5 symmetry functions, the curves are solid. (b) The energy scale is expanded in order to show the transition energies in the spectral region 60–80 cm^{-1}. The best agreement with the experimental line position is achieved for $K=8.4\pm0.3$ cm^{-1}. Note the anticrossing of the vibronic levels $|\Gamma_5{:}\Gamma_5 00)$ and $|\Gamma_5{:}\Gamma_4 11)$.

TABLE IV. Energies and oscillator strengths of the allowed transitions originating from the ground state $|\Gamma_1{:}\Gamma_1 00)$, calculated from the Jahn-Teller model for the set of parameters reported in Eq. (6.1) in the text. The final level of each transition is indicated in the first column. The experimental values of the energies are also reported for comparison. E and M refer to electric and magnetic processes, respectively.

Final vibronic states	Calculated energy (cm^{-1})	Experimental energy (cm^{-1})	Oscillator strength $10^{+8}f$	
$\|\Gamma_4{:}\Gamma_4 00)$	18.6	18.6	1.46	M
$\|\Gamma_5{:}\Gamma_4 01)$	43.3		0.13	E
$\|\Gamma_4{:}\Gamma_4 10)$	46.6		0.09	M
$\|\Gamma_5{:}\Gamma_5 00)$	65.5	66	2.92	E
$\|\Gamma_4{:}\Gamma_4 02)$	68.7		0.0015	M
$\|\Gamma_5{:}\Gamma_4 11)$	74.4	74	2.2	E
$\|\Gamma_4{:}\Gamma_4 20)$	74.4		0.005	M

cm^{-1} induced by Jahn-Teller coupling between the closely spaced $|\Gamma_5{:}\Gamma_5 00)$ and $|\Gamma_5{:}\Gamma_4 11)$ levels. Further evidence of this coupling is the repulsive interaction between the vibronic states $|\Gamma_5{:}\Gamma_5 00)$ and $|\Gamma_5{:}\Gamma_4 11)$, which is illustrated by the anticrossing of the corresponding levels in Fig. 5.

On the other hand, one-phonon transitions predicted at 43.3 and 46.6 cm^{-1} and two-phonon transitions involving $|\Gamma_4{:}\Gamma_4 02)$ and $|\Gamma_4{:}\Gamma_4 20)$ states are not observed in the experimental spectra. This is not surprising since the strengths of these transitions calculated from the model are much weaker than those of the zero-phonon transitions (see Table IV).

Note in the above calculations we have taken $\rho=0.18$ cm^{-1} for the spin-spin interaction entering Eq. (4.2). This value was calculated by Watson and Blume[16] for the ^5D term with an accuracy of 5%. However, a larger value ($\rho=1$ cm^{-1}) was inferred from the analysis of spectroscopic data by Pryce[18] and by Ham and Slack.[19] It was pointed out by Vallin[4] that this larger value represents an effective spin-spin interaction which mimics the effect of the spin-orbit interaction with higher terms of $3d^6$ configuration.

Since the value of ρ to be used in our present model is not unambiguously determined, we have also calculated the FIR spectrum for the value $\rho=1$ cm^{-1}. Calculated energies of the optical transitions differ by less than 0.1% from those reported in Table IV when using the set of parameters $Dq=-248$ cm^{-1}, $K=8.4$ cm^{-1}, $\hbar\omega=28$ cm^{-1}, and $\lambda=-90.55$ cm^{-1}. The oscillator strengths differ by less than 2% from the values given in Table IV. Therefore the change of the spin-spin interaction coefficient is equivalent to a renormalization of the spin-orbit parameter which varies from $\lambda=-101.9$ cm^{-1} (for $\rho=0.18$ cm^{-1}) to $\lambda=-90.55$ cm^{-1} (for $\rho=1$ cm^{-1}). But this change does not affect the excellent numerical agreement between the calculated and experimental spectra.

VII. PHONON TRANSITIONS

Besides the electronic transition discussed above, the FIR absorption spectra of CdTe and $Cd_{1-x}Fe_xTe$ alloys contain two absorption lines at 53 and 71.5 cm^{-1} which are intensified at high temperature (Fig. 2). These lines are attributable to phonon absorption processes.

The peak at 71.5 cm^{-1} having the same intensity in the spectrum of CdTe and $Cd_{1-x}Fe_xTe$ is a characteristic feature of the lattice. We ascribe this line to a two-phonon absorption process involving the transverse acoustic mode at the X point of the Brillouin zone with the energy $\hbar\omega=35\pm0.5$ cm^{-1}.[6] The conservation law of the wave vectors in the absorption process implies that the two absorbed TA(X) phonons propagate in opposite directions, while the one-phonon absorption process is forbidden. This explains why no absorption peak occurs at 35 cm^{-1}.

The feature at 54 cm^{-1} occurs only in the ternary compounds. This structure is most likely due to a quasilocal mode of Fe in CdTe as reported by Lu *et al.*[20] The fact that this absorption peak is proportional to the Fe composition (Fig. 2) and does not exist in pure CdTe strongly supports this interpretation.

VIII. CONCLUSION

We have studied the influence of the Jahn-Teller effect on ^5E electron orbital states of Fe^{2+} and $Cd_{1-x}Fe_xTe$ semimagnetic semiconductors. The vibronic states resulting from the electron-phonon coupling with the E modes are determined accurately. Optical transitions between vibronic states account quantitatively for the low-temperature FIR absorption lines for a Jahn-Teller energy $E_{JT}=2.5$ cm^{-1} and with the phonon energy $\hbar\omega=28$ cm^{-1} of the TA(L) mode in quite good agreement with the neutron-scattering data. We are thus in the situation of the dynamical Jahn-Teller effect ($E_{JT}\ll\hbar\omega/2$) where a static distortion does not occur. This value of $\hbar\omega$ is quite different from those used by Vallin[4] and by Vogel and Rivera-Iratchet[5] (38 and 51 cm^{-1}, respectively).

ACKNOWLEDGMENTS

The authors express their thanks to Professor J. Blinowski of Warsaw University (Poland) and M. Lannoo from Institut Superieur d'Electronique du Nord in Lille (France) for enlightening discussions. The authors gratefully acknowledge Madame N. Valignat, Service CMTC de l'Institut National Polytechnique (Grenoble), for making electron microprobe analysis.

*Permanent address: Institut of Physics, Polish Academy of Sciences, Al. Lotnikow 32, Warsaw, Poland.

[1]G. A. Slack, F. S. Ham, and R. M Chrenko, Phys. Rev. **152**, 376 (1966).

[2]G. A. Slack, S. Roberts, and J. T. Vallin, Phys. Rev. **187**, 511 (1969).

[3]J. P. Mahoney, C. C. Lin, and F. Dorman, J. Chem. Phys. **53**, 4286 (1970).

[4]J. T. Vallin, Phys. Rev. B **2**, 2390 (1970).

[5]E. E. Vogel and J. Rivera-Iratchet, Phys. Rev. B **22**, 4511 (1980).

[6]J. M. Rowe, R. M. Nicklow, D. L. Price, and K. Zanio, Phys. Rev. B **10**, 671 (1974).

[7]J. S. Griffith, *The Theory of Transition Metal Ions* (Cambridge University Press, New York, 1961), p. 204.

[8]G. F. Koster, J. O. Dimmock, R. G. Wheeler, and H. Statz, *Properties of the Thirty-Two Point Groups* (MIT Press, Cambridge, MA, 1963).

[9]J. Bourgoin and A. M. Lannoo, *Point Defects in Semiconductors II, Experimental Aspects* (Springer-Verlag, Berlin, 1983), p. 9.

[10]A. M. Stoneham and M. Lannoo, J. Phys. Chem. Solids **30**, 1769 (1969).

[11]F. S. Ham, Phys. Rev. **166**, 307 (1968).

[12]R. Loudon, Proc. R. Soc. (London) **84**, 379 (1964).

[13]C. Testelin, Thèse de doctorat de l'Université de Paris 6 (unpublished).

[14]See, for example, D. L. Dexter, in *Solid State Physics,* edited by F. Seitz and D. Turnbull (Academic, New York, 1959), Vol. 6, p. 353.

[15]G. A. Slack, S. Roberts, and F. S. Ham, Phys. Rev. **155**, 170 (1967).

[16]R. E. Watson and M. Blume, Phys. Rev. **139**, A1209 (1965).

[17]J. S. Griffith, *The Theory of Transition Metal Ions* (Cambridge University Press, New York, 1961), p. 437.

[18]M. H. L. Pryce, Phys. Rev. **80**, 1107 (1950).

[19]F. S. Ham and G. A. Slack, Phys. Rev. B **4**, 777 (1971).

[20]W. Lu, H. J. Ye, Z. Y. Yu, S. Y. Zhang, Y. Fu, W. L. Zu, S. C. Shen, and W. Giriat, Phys. Status Solidi B **147**, 767 (1968).